Investigation of Sr-based perovskites for redox-type thermochemical energy storage media at medium-high temperature

Xiaoyu Chen[a], Mitsuhiro Kubota[a*], Seiji Yamashita[b], Hideki Kita[a]

[a]Nagoya University, Graduate school of Engineering, Department of Chemical Systems Engineering, Nagoya 4648603, Japan

[b]Nagoya University, Graduate school of Engineering, Department of Materials Process Engineering, Nagoya 4648603, Japan

Abstract:

Thermochemical heat storage system exhibits extraordinary properties compared with sensible or latent heat storage system. Owing to the versatility of perovskite, Sr-based perovskites were investigated for redox-type thermochemical energy storage at medium-high temperature. In this study, $SrCoO_{3-\delta}$, $SrFeO_{3-\delta}$ and $SrMnO_{3-\delta}$ were prepared via a modified Pechini method. The oxidation enthalpy of each sample was measured using a combination of tubular furnace and DSC. Composition analysis, redox and cyclability tests revealed that $SrFeO_{3-\delta}$ possesses favorable behavior validating the design principles.

Keywords: Thermochemical energy storage; Sr-based perovskite; medium-high temperature

1. Introduction

Recently, due to the increasing global demand for energy and exhaustion of fossil fuel resources, there has been a greater focus on technology for solar and other renewable energy technologies. In the field of solar energy, concentrating solar power (CSP) plants represent the most effective form of solar energy conversion. Suffering from the problem of solar energy intermittency, excellent storage systems are needed to make continuous operation possible. As for now, the heat storage systems can be classified into sensible, latent, and thermochemical heat storage (TCS) system[1], of which TCS exhibits the most favorable properties, such as improved energy storage density, a wider range of operational temperature[2] and theoretically unlimited distance of transportation[3].

Redox type TCS system is based on reduction-oxidation reaction of metal oxide, as seen in Eq. (1). Driven by thermal energy, reduction (charge) process was conducted. When energy is later required, the metal oxides in their reduced state could re-oxidize in oxygen and release heat. Theoretically, it does not require a tank for the storage of gaseous products as oxygen can be extracted or released from the atmosphere.

$$\mathrm{MO}_{oxidized\ state} + \Delta H_r \rightleftharpoons \mathrm{MO}_{reduced\ state} + O_2 \quad (1)$$

Unlike traditional redox pairs, such as BaO_2/BaO[4], CuO/Cu_2O[5], Co_3O_4/CoO[6,7,8], Fe_2O_3/Fe_3O_4[9] and Mn_2O_3/MnO[10], perovskite oxides (ABO_3) do not encounter a discrete structural phase change during the redox process [Eq. (2)].

$$\mathrm{ABO}_{3-\delta_i}(s) + \Delta H_r \rightleftharpoons \mathrm{ABO}_{3-\delta_f}(s) + \frac{\delta_f - \delta_i}{2}\mathrm{O}_2(g) \quad (2)$$

*Corresponding author. Email-address: kubota.mitsuhiro@material.nagoya-u.ac.jp

where δ_i ($\delta_i < 0.5$) is the initial oxygen nonstoichiometric, and δ_f ($\delta_f \leq 0.5$) is the nonstoichiometric value when the predetermined temperature is reached.

Crystal phase transformation implies severe lattice reorganization will occur, potentially damaging the long-term recyclability of the material. Therefore, perovskites are more appropriate for TCS system than traditional redox pairs. Furthermore, the reduction and oxidation of perovskites occur faster than traditional redox pairs mentioned above, which can be attributed to the faster O^{2-} diffusion in nonstoichiometric oxides. Typically, perovskite oxides can re-oxidize in the air within a few seconds[11]. However, the heat storage density of perovskite material might be restricted by the absence of obvious crystal phase change.

Pioneering this work, Babiniec et al. investigated $La_xSr_{1-x}Co_yM_{1-y}O_{3-\delta}$ (M=Mn, Fe) perovskite materials as thermochemical energy storage media for CSP system in 2015[12]. Actually, $La_xSr_{1-x}Co_yM_{1-y}O_{3-\delta}$ can be regarded as $SrCoO_{3-\delta}$ doped by La, Mn and Fe. Increasing La concentration resulted in a lattice distortion away from the ideal cubic structure, which represented the highest redox capacity. Later, they reported the highest storage capacity (ΔH=390 kJ/kg) of perovskites until now, by using doped calcium manganites ($CaB_xMn_{1-x}O_{3-\delta}$, B=Al, Ti)[13].

Recently, Mastronardo et al. investigated $CaFe_xMn_{1-x}O_{3-\delta}$ (x = 0.1, 0.3) for thermochemical heat storage[14]. The introduction of 0.1 Fe prevented the decomposition of $CaMnO_3$ up to 1200 °C at pO_2 = 0.008 atm and increased the heat storage capacity into 344 kJ/kg. While $CaFe_{0.3}Mn_{0.7}O_{3-\delta}$ exhibits a higher oxygen exchange capacity, they claimed that the lower enthalpy accompanying the change in oxidation state resulted in a diminished heat storage capacity of 221 kJ/kg.

Zhang et al. reported Ba and Sr series perovskites for thermochemical energy storage[15]. They claimed that oxygen monoatomic ion of perovskites released from the crystal lattice is not subjected by a single energy threshold and results in an inconspicuous DSC peak during reduction and oxidation. Although Sr-based perovskites are already reported by Zhang et al.[15], detailed studies on energy storage density are lacking due to the limitation of DSC apparatus.

Currently, TCS technology is primarily applied for solar energy utilization and recycle. However, other thermal technology fields, such as steel industry, electric vehicle, and seasonal indoor heating, also require advanced TCS technology. In practice, such applications cannot be operated under excessively high-temperature condition and volume restrictions for heat storage equipment may exist. Although most researches in this filed focus on the high temperature, the development of medium-high temperature heat storage technology remains stagnant, resulting in wasted energy resources as well as gaps in TCS research. The utilization of thermal energy is always a challenge in the field of renewable energy; in particular, the exergy of thermal energy is limited as the temperature decreasing, making that energy is more difficult to capture.

A few principles for medium-high temperature redox-type thermochemical energy storage deign are summarized below:

I. Fast reaction kinetics; either reduction or oxidation.
II. Can be operable in the medium-high temperature range.
III. Appropriated operational oxygen partial pressure (A high or low pO_2 requires more energy input).
IV. Sufficient thermochemical heat storage capacity.
V. Cyclability and durability.
VI. Affordable raw materials.
VII. Low toxicity.

Herein, the composition analysis, redox ability and cyclability of Sr-based perovskite were investigated. Oxidation enthalpy was investigated in particular by a combination of tubular furnace and DSC analysis.

2. Experimental approach

2.1 Synthesis

$SrBO_{3-\delta}$ (B=Mn, Fe, Co, Ni, Cu) perovskite was synthesized by a modified Pechini method[16]. Stoichiometric amounts of nitrate salts $Sr(NO_3)_2$ (98%, FUJIFILM Wako Pure Chemical Corporation), $Mn(NO_3)_2{\cdot}6H_2O$ (98%, FUJIFILM Wako Pure Chemical Corporation), $Fe(NO_3)_3{\cdot}9H_2O$ (99%, FUJIFILM Wako Pure Chemical Corporation), $Co(NO_3)_2{\cdot}6H_2O$ (98%, FUJIFILM Wako Pure Chemical Corporation), $Ni(NO_3)_2{\cdot}6H_2O$ (98%, FUJIFILM Wako Pure Chemical Corporation), and $Cu(NO_3)_2{\cdot}3H_2O$ (98%, FUJIFILM Wako Pure Chemical Corporation) were dissolved in deionized water, then citric acid was added to the solution at a ratio of 1:2 (cation : citric acid). Ethylene glycol was introduced as a reactant with citric acid, then adjusted the pH value to around 9 with ammonia solution subsequently. The solution was dried and pre-calcined at 500 °C for 1h in air to remove all the organic components. After grounding, these powders were pelletized with a 25 mm die at 30 MPa, then pellets were heated to 1200 °C for 5 hours in air. In order to preserve the metastable brownmillerite (reduction state) phase of perovskite until XRD analysis was performed, a few samples were quenched by liquid N_2. The remaining samples were cooled at room temperature. For convenience, the quenched samples are denoted as Q-$ABO_{3-\delta}$ and the samples without quenching are denoted as NQ-$ABO_{3-\delta}$.

2.2 Structural characterization

The pre-calcined sample, Q-$ABO_{3-\delta}$ and NQ-$ABO_{3-\delta}$ sample were investigated using X-ray diffraction (XRD) (SmartLab, Rigaku) with Cu Kα radiation (λ = 0.15418 nm, 40 kV – 25 mA). Crystalline phases were analyzed using PDXL2 (Rigaku Data Analysis Software).

2.3 TG analysis and SEM morphology

Three thermogravimetric analysis programs were performed for this study. For the first program, the redox capacity and mass change of the NQ-$ABO_{3-\delta}$ and Q-$ABO_{3-\delta}$ families were evaluated. The

primary redox characterization of the NQ-$ABO_{3-\delta}$ and Q-$ABO_{3-\delta}$ families was tested using pellet fragments (~20mg) in a HITACHI STA7300. This experiment could not determine the absolute δ values of each sample, but provided an appropriate standard for comparing different families. The first program consisted of two cycles. The "break-in" cycle aim to removing any impurity (i.e. adsorbed species on the surface of the sample) [12,17,18] and eliminating the quenching effect. The initial mass was recorded at 100 °C, and the sample was heated up to 1000 °C holding for 1 h then re-oxidized in the air while cooled to 100 °C for 90 min. This investigation was vital for screening the best candidates for further study. The second program acted as a "pre-experiment" aims to obtaining an oxidation rate of the reduced perovskites at room temperature. This ensured the validity of combining a tubular furnace and DSC analysis. The third program was set up for cyclability and durability tests. The SEM morphology was also studied using as-prepared, 1 cycle and 10 cycles samples. Details on each TG program will be presented in later section.

2.4 Oxidation enthalpy measurement

To measure oxidation enthalpy, NQ-$ABO_{3-\delta}$ samples were heated to 1000 °C in an argon flow using tubular furnace to obtain the most reduced $ABO_{2.5}$ brownmillerite phase, then cooled down to the room temperature also in a protective argon flow. Isothermal oxidation method was performed for $SrCoO_{3-\delta}$ and $SrFeO_{3-\delta}$. After heating to the appropriate temperature under N_2 protection, the gas was changed to air when target temperature was stable. The exothermic signal was detected using DSC apparatus (DSC-60, Shimadzu Corp.). The oxidation enthalpy of $SrMnO_{3-\delta}$ was measured using a non-isothermal oxidation method.

3. Results and discussion

3.1 Synthesis mechanism and characterization of composition

The preparation schematic of Sr-based perovskites via Pechini method was shown in Figure 1.

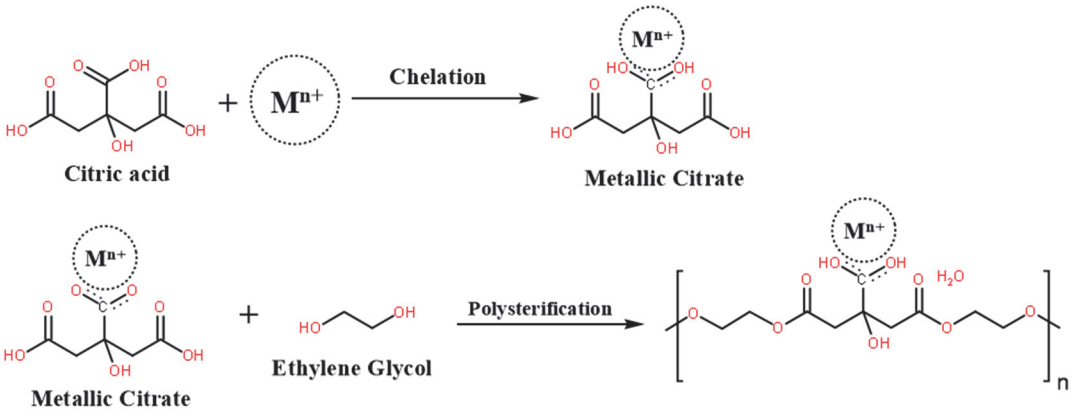

Figure 1. Preparation schematic.

Metallic cations were initially chelated with citric acid. With the aid of polyalcohol, the corresponding metallic citrates were cross-linked to form a gel through esterification. The organic compositions were removed after pre-calcine process, and the cations were subsequently oxidized at high temperature to form a perovskite structure.

Although $SrNiO_{3-\delta}$ and $SrCuO_{3-\delta}$ perovskite were also prepared using Pechini method, pure $SrNiO_{3-\delta}$ and $SrCuO_{3-\delta}$ perovskite were not obtained in this study because of their instability in normal condition[19,20]. Moreover, the complex synthesis conditions do not satisfy the design principles and unsuitable for practical application. Therefore, only $SrCoO_{3-\delta}$, $SrFeO_{3-\delta}$ and $SrMnO_{3-\delta}$ were considered for further study.

To confirm the validity of Pechini methods, XRD analysis of pre-calcined, NQ-$ABO_{3-\delta}$ and Q-$ABO_{3-\delta}$ samples were performed. The results are summarized in Table 1 and typical XRD pattern of NQ-$ABO_{3-\delta}$ and Q-$ABO_{3-\delta}$ samples are presented in Figure 2.

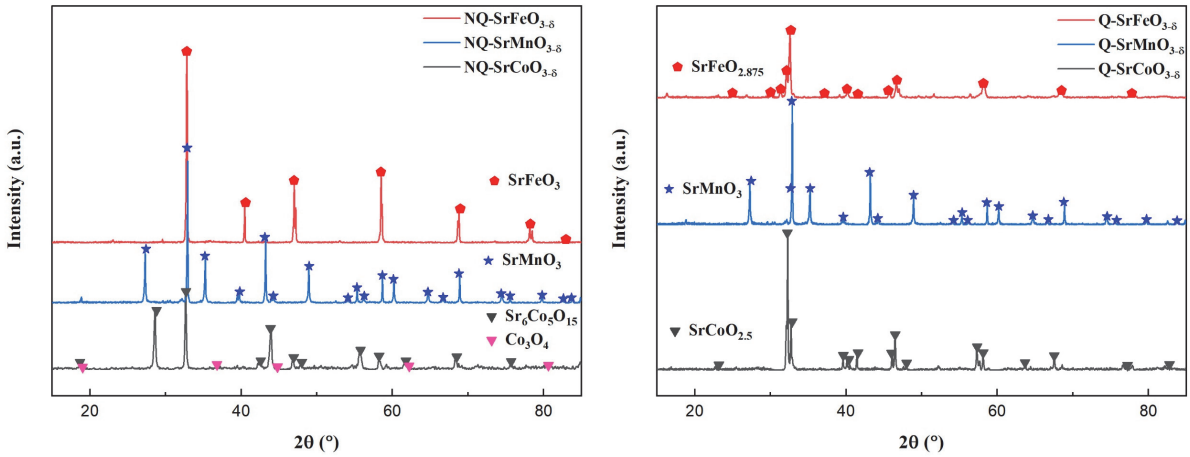

Figure 2. XRD patterns of NQ-ABO_3 and Q-ABO_3 samples.

The XRD results of pre-calcined samples coincide with the mechanism introduced in Figure 1, but interestingly, Sr tends to create two kinds of simple substance rather than oxides. Conversely, transition metal elements readily generated oxides with relatively high valences, which are very close to target perovskites. As temperature continually increases, these Sr simple substances have the ability to reduce the cationic position of certain transition oxides. Therefore, the Sr cation acts as the A-site and transition metallic cation settles at B-site of perovskites.

The phase composition of the unquenched samples (NQ-$SrCoO_{3-\delta}$, NQ-$SrFeO_{3-\delta}$, and NQ-$SrMnO_{3-\delta}$) were analyzed using XRD. After compared with standard PDF card, it was observed that instead of the predicted $SrCoO_3$ phase, NQ-$SrCoO_{3-\delta}$ exhibited a $Sr_6Co_5O_{15}$ phase that the molar ratio of Sr and Co is not equal to 1:1. Previous evidence suggests that during room temperature cooling of $SrCoO_{3-\delta}$ after the Pechini method, it will decompose into $Sr_6Co_5O_{15}$ and a small amount of Co_3O_4. Based on the synthesis mechanism of pre-calcined samples, there are two possible explanations for this result:

A. when cooling at room temperature, a small amount of Co was decomposed from $SrCoO_{3-\delta}$ then slowly oxidized in air, while remaining $SrCoO_{3-\delta}$ was evolved into more stable $Sr_6Co_5O_{15}$ phase; **B.** during the cooling process, $SrCoO_3$ was generated first, and a small amount of Sr was decomposed from $SrCoO_{3-\delta}$ then reacted with the undecomposed $SrCoO_{3-\delta}$ to form $Sr_6Co_5O_{15}$. Irrespective of the mechanism, the XRD results suggested $Sr_6Co_5O_{15}$ is more stable than $SrCoO_3$ at room temperature, making it difficult to synthesize and use in practical applications. The Sr-Co-O phase diagram[21] shows that when temperature was lower than 1150 K, it was impossible to form $SrCoO_3$ perovskite even if the mole ratio of raw materials was 1:1.

Conversely, $SrFeO_{3-\delta}$ presented continued phase from high temperature to room temperature. Nonetheless, even unquenched sample shows unsaturated phase mainly because the dense pelletization of sample may obstruct oxygen diffusion, the inner part cannot acquire enough oxygen.

The metastable brownmillerite phase can be obtained using the quenching method. However, Q-$SrFeO_{3-\delta}$ also consists of $SrFeO_{2.875,}$ maintaining a relatively larger δ value. This suggested that even sample was "frozen" by the quenching method, but it will still slowly oxidize over time. It is interesting to notice that the quenching effect of $SrMnO_{3-\delta}$ has not been detected, which can be attributed to stronger Mn-O bond that needs higher temperature to release lattice oxygen. Moreover, $SrMnO_3$ shows hexagonal structure instead of standard ABO_3 perovskite cubic structure, leading its redox behavior, viz. oxygen exchange capacity, which deviates from another two[22].

Table 1. Main phase, crystal structure and PDF-code of each sample.

Sample	Main phase	Crystal Structure	PDF-#
Pre-calcined-$SrCoO_{3-\delta}$	α-Sr, γ-Sr, $Co_{2.62}O_4$	(-)	(-)
Pre-calcined-$SrFeO_{3-\delta}$	α-Sr, γ-Sr, Fe_3O_4	(-)	(-)
Pre-calcined-$SrMnO_{3-\delta}$	α-Sr, γ-Sr, Mn_2O_3	(-)	(-)
NQ-$SrCoO_{3-\delta}$	$Sr_6Co_5O_{15}$	Trigonal, *R32 (155)*	00-060-0757
NQ-$SrFeO_{3-\delta}$	$SrFeO_3$, $SrFeO_{2.75}$	Cubic, *Pm-3m (221)* Orthorhombic, *Cmmm (65)*	01-070-6802, 01-070-5777
NQ-$SrMnO_{3-\delta}$	$SrMnO_3$	Hexagonal, *P63/mmc (194)*	01-084-1612
Q-$SrCoO_{3-\delta}$	$SrCoO_{2.5}$	Orthorhombic, *Ima2 (46)*	01-078-5502
Q-$SrFeO_{3-\delta}$	$SrFeO_{2.5}$, $SrFeO_{2.875}$	Orthorhombic, *Icmm (74)* Tetragonal, *I4/mmm (139)*	01-070-0836, 00-059-0638
Q-$SrMnO_{3-\delta}$	$SrMnO_3$	Hexagonal, *P63/mmc (194)*	01-084-1612

3.2 Redox behavior

The redox behavior of NQ-$ABO_{3-\delta}$ and Q-$ABO_{3-\delta}$ families were determined using TGA. Figure 3 shows the profile of TGA program and mass change of each sample. $SrCoO_{3-\delta}$ and $SrFeO_{3-\delta}$ exhibited very similar redox behavior when heated to 1000 °C in the atmospheric ambient, while $SrMnO_{3-\delta}$ showed inactivity under these conditions. Because some adsorbed species may remain on the surface of the sample, the first cycle is used to diminish the effect of impurities. The initial mass of the second cycle was used as the initial mass of each sample at a time of 210 min.

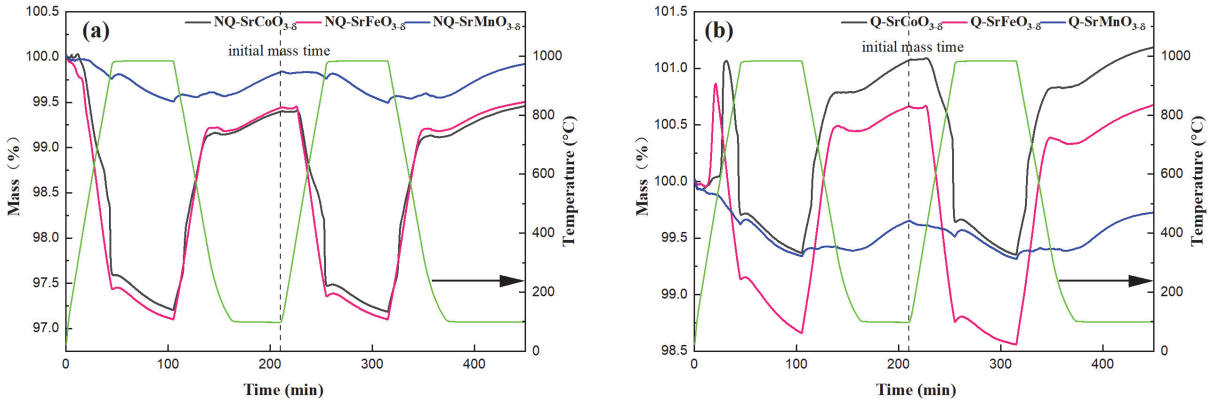

Figure 3. Redox behavior of (a) NQ-$ABO_{3-\delta}$ and (b) Q-$ABO_{3-\delta}$ families.

The changes in mass of unquenched $SrCoO_{3-\delta}$, $SrFeO_{3-\delta}$ and $SrMnO_{3-\delta}$ samples are 2.11%, 2.34% and 0.34%, respectively. The changes in mass of quenched $SrCoO_{3-\delta}$, $SrFeO_{3-\delta}$ and $SrMnO_{3-\delta}$ samples were slightly lower (1.72%, 2.11% and 0.33%, respectively). The change in δ, namely Δδ, can be calculated easily using Eq. (3):

$$\Delta\delta = \frac{\Delta m \cdot MW_{ABO3}}{m_{initial} \cdot MW_O} \tag{3}$$

where Δm is the change in mass, $m_{initial}$ is the initial mass, MW_{ABO3} is the molecular weight of perovskite ($\delta = 0$), MW_O is the molecular weight of monoatomic oxygen. The results for Δδ are listed in Table 2.

It is interesting to notice that after quenching process the redox behavior of $ABO_{3-\delta}$ was slightly worse than those unquenched samples. This is mainly due to irreversible damage caused to $ABO_{3-\delta}$ during the quenching process; being unable to return to most oxidized state leads to a narrow range of mass change. In particular, the Q-$ABO_{3-\delta}$ families show rapid mass change behavior in the first cycle, around 700 °C and 400 °C for $SrCoO_{3-\delta}$ and $SrFeO_{3-\delta}$, respectively. By quenching, the perovskite sample can be "frozen" at reduced state until it returns to room temperature. When "frozen" perovskite was heated again, the oxidation rate was faster. As presented in Figure 3 (b), when a certain temperature was reached, around 800 °C for $SrCoO_{3-\delta}$ and 500 °C for $SrFeO_{3-\delta}$, Q-$ABO_{3-\delta}$ almost return to the initial mass. However, as temperature keeps increasing the reduction behavior was observed. Although the reduction reaction occurs during the entire heating process, the reduction rate is lower than the

oxidation rate until a certain temperature is reached. Nonetheless, unlike the other perovskites, $SrMnO_{3-\delta}$ did not exhibit an obvious quenching effect except for a slight variation in the mass change.

Table 2. The value of Δδ (Mean value ± standard deviation) for No-Quench and Quenched families.

Experiment Condition	$SrCoO_{3-\delta}$	$SrFeO_{3-\delta}$	$SrMnO_{3-\delta}$
No-Quench	0.266 ± 0.007	0.279 ± 0.003	0.049 ± 0.006
Quenched	0.199 ± 0.008	0.262 ± 0.007	0.048 ± 0.007

Actually, in the case of $SrCoO_{3-\delta}$ and $SrFeO_{3-\delta}$, their redox behaviors are quite different in a sense due to their own property. The mass change of $SrFeO_{3-\delta}$ seems like a linear function in the temperature range from 400 °C to 1000 °C either reduction or oxidation. This property can exist over two cycles, which can be demonstrated by cyclability test. $SrCoO_{3-\delta}$, on the other hand, represents more complicated reduction behavior. This behavior can be classified into broken line function, with a change in slope at approximately 900 °C. It can be attributed to the variety of Sr-Co-O ternary component phase. Ondřej Jankovský et al.[21] previously investigated the detailed phase composition of Sr-Co-O. According to Sr-Co-O phase diagram, at a temperature below 877 °C, Sr and Co can only create quasi-one-dimensional $Sr_6Co_5O_{15}$[23] rather than the $SrCoO_{3-\delta}$ perovskite structure. These results also show perfect consistency with ours. From another point of view, varied phase change during the redox process seems unfavorable to reactor design because of the instability of kinetics. Even when the $SrMnO_{3-\delta}$ was heated up to 1000 °C, it remained in a relatively high oxidation state. In the supplementary experiment performed by Zhang et al.[15], despite heating $SrMnO_{3-\delta}$ perovskite to 1150 °C in an Ar atmosphere, namely reduced in an extremely low oxygen partial pressure, it only exhibited a mass change of less than 2%. This indicates that $SrMnO_{3-\delta}$ may possess a large reduction enthalpy; the estimated value was reported by other authors[24,25], but in terms of heat storage at medium-high temperature, the rigorous operating conditions pose some problems.

3.3 Oxidation enthalpy estimate

To confirm that the oxidation rate in the ambient condition of the reduced sample was slow enough for DSC measurement, a pre-experiment was performed with the result shown in Figure. S1. The NQ-$ABO_{3-\delta}$ family was heated to 1000 °C in a N_2 atmosphere to obtain reduced samples, then gas was changed into synthesized air while temperature was fixed at 100 °C to determine the oxidation rate under normal condition. The values of Δδ in N_2 atmosphere and air are listed in Table S1. To study the thermochemical heat storage capacity per unit volume, the density of each sample was measured using helium pycnometer method, with results of 5.70 g/cm^3 for $SrCoO_{3-\delta}$, 5.79 g/cm^3 for $SrFeO_{3-\delta}$ and 6.82 g/cm^3 for $SrMnO_{3-\delta}$.

3.3.1 Oxidation enthalpy of $Sr(Co,Fe)O_{3-\delta}$

According to the calculation results from Figure. S1, $SrCoO_{3-\delta}$ and $SrFeO_{3-\delta}$ can be almost reduced into $ABO_{2.5}$ brownmillerite phase, and the changes in δ for $SrCoO_{3-\delta}$ and $SrFeO_{3-\delta}$ were so small that they can be ignored while gas was changed into air. Oxidation state samples were subjected to heat treatment using tubular furnace to obtain reduced samples. Then reduced samples were heated to appropriate temperature in N_2 protection, the gas was changed to air, and the DSC exothermic peak was monitored. This is known as the isothermal oxidation method. Typical DSC results were shown in Figure 4.

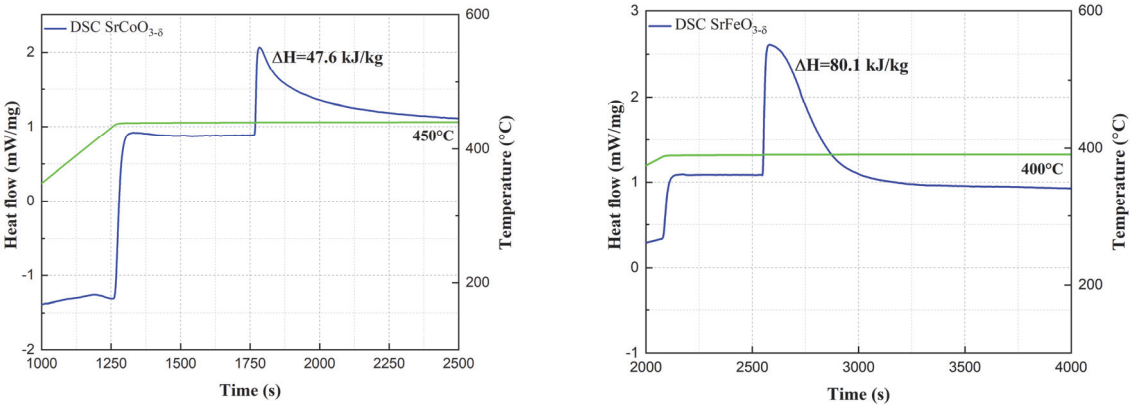

Figure 4. The DSC curve for reduced $Sr(Co,Fe)O_{3-\delta}$ with isothermal oxidation method.

An appropriate oxidation temperature is crucial for each reduced sample due to the temperature and oxygen partial pressure sensitivity of perovskite materials. Excessively high oxidation temperature may result in incomplete oxidation, as high temperature also promotes reduction reaction. However, at insufficient temperature, the oxidation reaction may be too tardy to generate visible peak. Hence, the oxidation temperature for $SrCoO_{3-\delta}$ and $SrFeO_{3-\delta}$ are 450 °C and 400 °C (program temperature), respectively.

Among the DSC results, only $SrFeO_{3-\delta}$ showed the intact exothermic peak, while $SrCoO_{3-\delta}$ represented semi-peak or vaulted peak. Interestingly, the DSC curve of $SrCoO_{3-\delta}$ has two-level baselines before and after reaction, which suggested a change in the specific heat capacity of $SrCoO_{3-\delta}$. This can be attributed to the formation of $Sr_6Co_5O_{15}$ we discussed previously. Despite the similarity of the redox behavior of $SrCoO_{3-\delta}$ and $SrFeO_{3-\delta}$ the oxidation enthalpy of $SrCoO_{3-\delta}$ is 47.6 ± 5.7 kJ/kg-ABO_3 (270.5 ± 32.3 kJ/L) which slightly smaller than 81.7 ± 3.4 kJ/kg-ABO_3 (473.5 ± 20.0 kJ/L). In addition, it is worth noting that the exothermic peak measured by DSC is usually smaller than the real value, which is mainly due to the inevitable heat loss.

3.3.2 Oxidation enthalpy of $SrMnO_{3-\delta}$

It was found that $SrMnO_{3-\delta}$ appears to have a significant oxygen affinity. Even when the reduced $SrMnO_{3-\delta}$ was heated to 500 °C in N_2 atmosphere (extreme low oxygen partial pressure), the reduced $SrMnO_{3-\delta}$ still re-oxidized in 30 min. As seen in Figure. S2, the reduced $SrMnO_{3-\delta}$ exhibits similar oxidation behavior in N_2 or Air. For this reason, a non-isothermal oxidation method was adopted. The reduced $SrMnO_{3-\delta}$ was heated at a fixed heating rate (10°C/min) in air. After integrated the exothermic peak, the oxidation enthalpy was found to be 25.6 ± 5.8 kJ/kg-ABO_3 (230.3 ± 39.4 kJ/L). A typical pattern is shown in Figure 5.

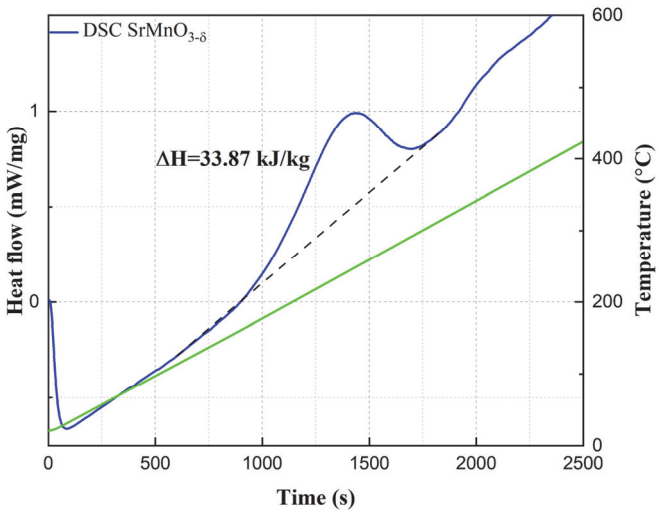

Figure 5. The DSC curve for reduced $SrMnO_{3-\delta}$ with non-isothermal oxidation method.

Since it was found that $SrMnO_{3-\delta}$ can only reach a small Δδ (from Figure. S2, Δδ only reached 0.1), even under high temperature and low pO_2 condition, its oxidation enthalpy was not satisfactory. On the contrary, it shows an unusual stability, suggesting that $SrMnO_{3-\delta}$ may possess the highest oxidation enthalpy among the all Sr-based perovskites while its Δδ is sufficiently large. Unfortunately, because the relationship of Δδ and enthalpy is not always linear, it is difficult to predict the complete oxidation value by DSC method from only a single point. Vieten et al.[24] estimated the reaction enthalpy of $SrMnO_{3-\delta}$ (373 ± 55 kJ/mol-O_2) using Van't Hoff approach, but this method poses severe measurement uncertainties since only small mass changes were detected. It is worth noting that the unit they used (kJ/mol-O_2) means the amount of heat released when perovskite reacts with 1 mol of oxygen. In 2001, Rørmark et al.[26] measured the oxidation enthalpy of $SrMnO_{3-\delta}$ to be 293 ± 10 kJ/mol-O_2 and 73.3 ± 0.5 kJ/mol-Mn (~384.65 kJ/kg). Furthermore, comparing with the DFT-based data[27, 28, 29], the reaction enthalpy of $SrMnO_{3-\delta}$ is 340 kJ/mol-O_2. From the literature, $SrMnO_{3-\delta}$ does possess a larger reaction enthalpy, as expected from the design principles, but the high stability of $SrMnO_{3-\delta}$ in the range of 500-1000 °C results in practical difficulties. In conclusion, only $SrFeO_{3-\delta}$ was found to be able to operate under medium-high temperature conditions.

3.4 Cyclability test

$SrFeO_{3-\delta}$ was chosen for further cyclability test in 10 redox cycles, as shown in Figure 6. Aside from the first cycle not showing a satisfactory depth of reduction, the other cycles show an excellent cyclability in air. The large mass loss seen in the first cycle can be attributed to the desorption of water vapor or other adsorbed species. From this perspective, $SrFeO_{3-\delta}$ could return to the relatively high oxidation state, at a mass very close to the authentic initial mass, when temperature was cooled down to 100 °C.

As shown in Figure 7 (a-b), some $SrFeO_{3-\delta}$ agglomerated and generated relatively large particles whose size is over 20 μm. The agglomerated particles appear to have a terraced and exfoliated structure. In the magnified view, the terraced structure is distinct, with some small holes (about 1 μm) visible on the surface of particles. The point defects in crystal growth may play an important role in determining of surface morphology. For example, defects may accelerate the oxygen exchange rate due to the increment of surface area. However, after two cycles, only a small amount of the terraced structure remains, and the point defect can no longer be detected, as seen in Figure 7 (c-d). The 10 cycles result shown in Figure 7 (e-f) indicate that $SrFeO_{3-\delta}$ exhibits severe sintering, and the terraced structure no longer exists. Some holes can be distinguished, but they should be considered as incomplete sintering instead of point defects. Surprisingly, even suffer from the significant sintering, the redox behavior of $SrFeO_{3-\delta}$ is still adequate.

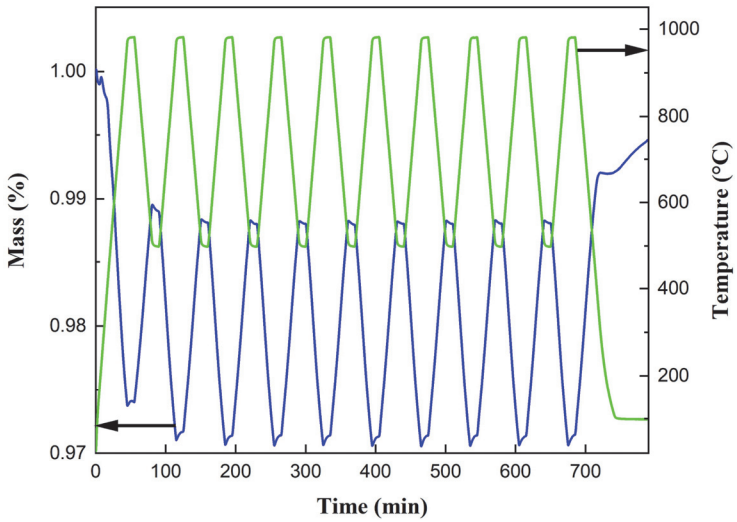

Figure 6. The 10 redox cycles test of $SrFeO_{3-\delta}$.

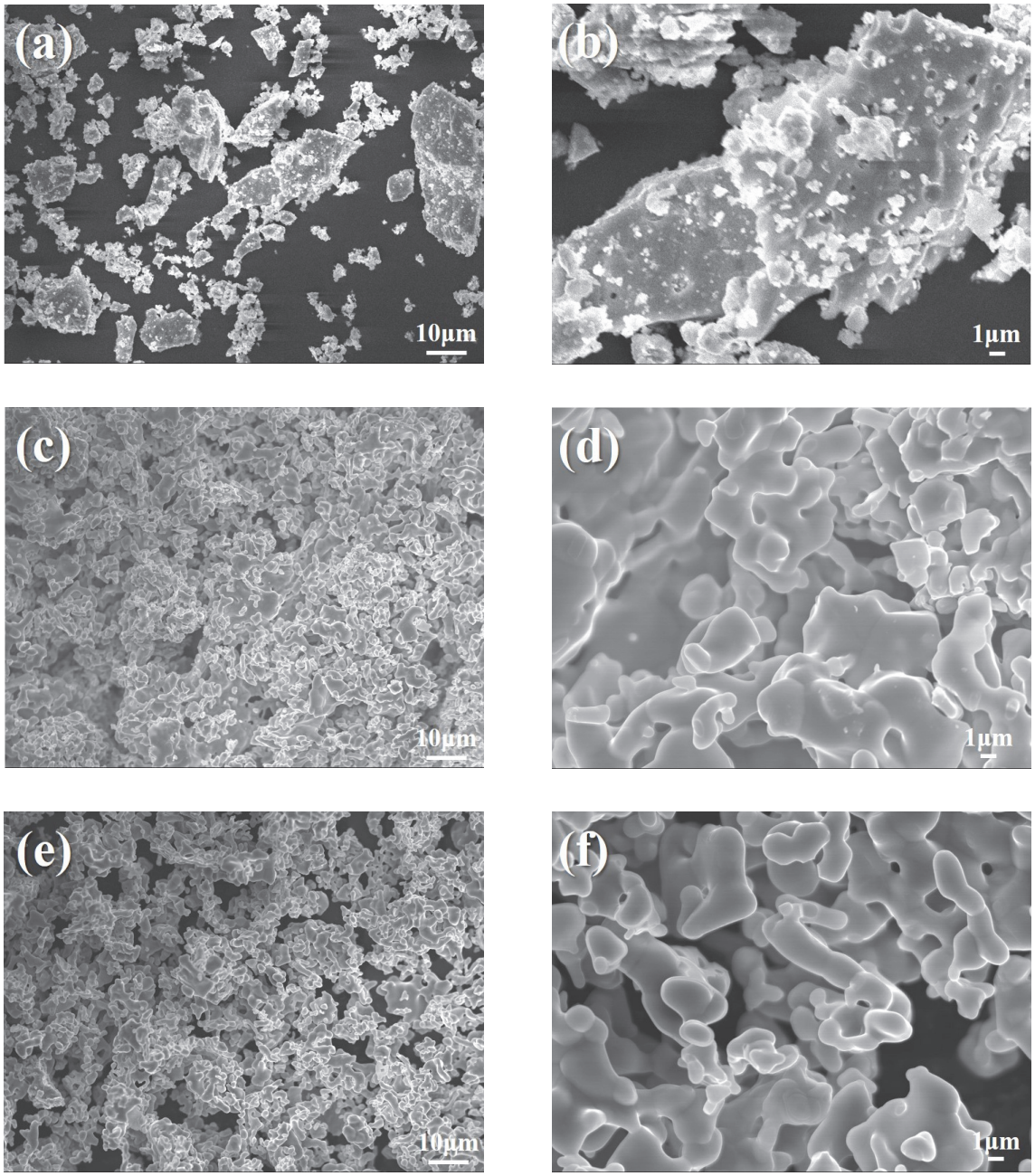

Figure 7. SEM images of $SrFeO_{3-\delta}$: (a-b) for as-prepared sample, (c-d) for 2-cycles sample and (e-f) for 10-cycles sample.

4. Conclusions

In this research, Sr-based transition metal perovskites were prepared for thermochemical energy storage at medium-high temperature. Owing to the instability of $SrCuO_{3-\delta}$ and $SrNiO_{3-\delta}$, only $SrCoO_{3-\delta}$, $SrFeO_{3-\delta}$ and $SrMnO_{3-\delta}$ were successfully formed via the modified Pechini method. The "frozen" samples were obtained using quenching method to investigate their crystal structure. The structure of $SrMnO_{3-\delta}$ is deviate from the ideal perovskite cubic structure and shows diminished redox capacity at

1000 °C, even in the N_2 atmosphere. However, several reports have shown that $SrMnO_{3-\delta}$ may possess the highest reaction enthalpy (300~400 kJ/mol-O_2) among three candidates due to the stronger Mn-O bonds and non-cubic structure.

Although $SrCoO_{3-\delta}$ has very similar redox capacity to that of $SrFeO_{3-\delta}$, according to the phase diagram of Sr-Co-O, its variant phase transition is unfavorable to the TCS system. $SrCoO_{3-\delta}$, $SrFeO_{3-\delta}$ and $SrMnO_{3-\delta}$ were heated to 1000 °C to obtain reduced phase. After DSC measurement, the oxidation enthalpies of each sample are 47.6 ± 5.7 kJ/kg-ABO_3 (270.5 ± 32.3 kJ/L), 81.7 ± 3.4 kJ/kg-ABO_3 (473.5 ± 20.0 kJ/L) and 25.6 ± 5.8 kJ/kg-ABO_3 (230.3 ± 39.4 kJ/L), respectively. Theoretically, if all samples reach the same Δδ, the oxidation enthalpy will increase in the increase of element metallicity, which may be related to the difference of M-O bonds strength ($SrNiO_{3-\delta}$ and $SrCuO_{3-\delta}$ could also be considered as their M-O bonds are too weak to form).

Since $SrFeO_{3-\delta}$ exhibited excellent redox capacity, further cyclability tests were performed and their morphology was investigated by SEM. The result showed a good cyclability for 10 cycles even after sintering. In conclusion, $SrFeO_{3-\delta}$ meets the requirements for operation in moderate oxygen partial pressure and medium-high temperature range and possesses exceptional cyclability. However, the limited thermochemical energy storage capacity and reaction kinetics require further investigation.

Acknowledgement

This research was supported by "Knowledge Hub Aichi", Priority Research Project from Aichi Prefectural Government, Japan

Reference

1. Carrillo, A. J., González-Aguilar, J., Romero, M. & Coronado, J. M. Solar Energy on Demand: A Review on High Temperature Thermochemical Heat Storage Systems and Materials. *Chem. Rev.* **119**, 4777–4816 (2019).
2. Kubota, M., Matsumoto, S. & Matsuda, H. Enhancement of hydration rate of LiOH by combining with mesoporous carbon for Low-temperature chemical heat storage. *Appl. Therm. Eng.* **150**, 858–863 (2019).
3. Pardo, P. *et al.* A review on high temperature thermochemical heat energy storage. *Renew. Sustain. Energy Rev.* **32**, 591–610 (2014).
4. Carrillo, A. J., Sastre, D., Serrano, D. P., Pizarro, P. & Coronado, J. M. Revisiting the BaO_2/BaO redox cycle for solar thermochemical energy storage. *Phys. Chem. Chem. Phys.* **18**, 8039–8048 (2016).
5. Deutsch, M. *et al.* High-Temperature Energy Storage: Kinetic Investigations of the CuO/Cu2O Reaction Cycle. *Energy and Fuels* **31**, 2324–2334 (2017).
6. Agrafiotis, C., Roeb, M., Schmücker, M. & Sattler, C. Exploitation of thermochemical cycles based

on solid oxide redox systems for thermochemical storage of solar heat. Part 1: Testing of cobalt oxide-based powders. *Sol. Energy* **102**, 189–211 (2014).

7. Agrafiotis, C., Roeb, M., Schmücker, M. & Sattler, C. Exploitation of thermochemical cycles based on solid oxide redox systems for thermochemical storage of solar heat. Part 2: Redox oxide-coated porous ceramic structures as integrated thermochemical reactors/heat exchangers. *Sol. Energy* **114**, 440–458 (2015).
8. Agrafiotis, C., Tescari, S., Roeb, M., Schmücker, M. & Sattler, C. Exploitation of thermochemical cycles based on solid oxide redox systems for thermochemical storage of solar heat. Part 3: Cobalt oxide monolithic porous structures as integrated thermochemical reactors/heat exchangers. *Sol. Energy* **114**, 459–475 (2015).
9. Block, T. & Schmücker, M. Metal oxides for thermochemical energy storage: A comparison of several metal oxide systems. *Sol. Energy* **126**, 195–207 (2016).
10. Lei, Q., Bader, R., Kreider, P., Lovegrove, K. & Lipiński, W. Thermodynamic analysis of a combined-cycle solar thermal power plant with manganese oxide-based thermochemical energy storage. *E3S Web Conf.* **22**, (2017).
11. Imponenti, L., Albrecht, K. J., Braun, R. J. & Jackson, G. S. Measuring Thermochemical Energy Storage Capacity with Redox Cycles of Doped-$CaMnO_3$. *ECS Trans.* **72**, 11–22 (2016).
12. Babiniec, S. M., Coker, E. N., Miller, J. E. & Ambrosini, A. Investigation of $La_xSr_{1-x}Co_yM_{1-y}O_{3-\delta}$ (M=Mn, Fe) perovskite materials as thermochemical energy storage media. *Sol. Energy* **118**, 451–459 (2015).
13. Babiniec, S. M., Coker, E. N., Miller, J. E. & Ambrosini, A. Doped calcium manganites for advanced high-temperature thermochemical energy storage. *Int. J. Energy Res.* **40**, 280–284 (2016).
14. Mastronardo, E., Qian, X., Coronado, J. M. & Haile, S. M. The favourable thermodynamic properties of Fe-doped $CaMnO_3$ for thermochemical heat storage. *J. Mater. Chem. A* **8**, 8503–8517 (2020).
15. Zhang, Z., Andre, L. & Abanades, S. Experimental assessment of oxygen exchange capacity and thermochemical redox cycle behavior of Ba and Sr series perovskites for solar energy storage. *Sol. Energy* **134**, 494–502 (2016).
16. Pechini, M. P. Method of Pre Parng Lead and Alkalne Earth Titanates and Nobates and Coat. *US Pat. 3,330,697* 2 (1967).
17. Ambrosini, A. *et al.* Synthesis and characterization of ferrite materials for thermochemical CO_2 splitting using concentrated solar energy. *ACS Symp. Ser.* **1056**, 1–13 (2010).
18. Ksepko, E. Perovskite-type Sr(Mn1-xNix)O3 materials and their chemical-looping oxygen transfer properties. *Int. J. Hydrogen Energy* **39**, 8126–8137 (2014).
19. Zinkevich, M. Constitution of the Sr-Ni-O system. *J. Solid State Chem.* **178**, 2818–2824 (2005).
20. Aicock, C. B. & Li, B. *Thermodynamic Study of the Cu-Sr-0 System*. *J Am CerOm Soc* vol. 73

(1990).

21. Jankovský, O., Sedmidubský, D., Vítek, J., Šimek, P. & Sofer, Z. Phase diagram of the Sr-Co-O system. *J. Eur. Ceram. Soc.* **35**, 935–940 (2015).

22. Curnan, M. T. & Kitchin, J. R. Effects of concentration, crystal structure, magnetism, and electronic structure method on first-principles oxygen vacancy formation energy trends in perovskites. *J. Phys. Chem. C* **118**, 28776–28790 (2014).

23. Botana, A. S. *et al.* Non-one-dimensional behavior in charge-ordered structurally quasi-one-dimensional $Sr_6Co_5O_{15}$. *Phys. Rev. B - Condens. Matter Mater. Phys.* **83**, 1–8 (2011).

24. Vieten, J. *et al.* Redox thermodynamics and phase composition in the system $SrFeO_{3-\delta}$ — $SrMnO_{3-\delta}$. *Solid State Ionics* **308**, 149–155 (2017).

25. Vieten, J. *et al.* Perovskite oxides for application in thermochemical air separation and oxygen storage. *J. Mater. Chem. A* **4**, 13652–13659 (2016).

26. Rørmark, L., Mørch, A. B., Wiik, K., Stølen, S. & Grande, T. Enthalpies of oxidation of $CaMnO_{3-\delta}$, $Ca_2MnO_{4-\delta}$ and $SrMnO_{3-\delta}$ - Deduced redox properties. *Chem. Mater.* **13**, 4005–4013 (2001).

27. Jain, A. *et al.* Formation enthalpies by mixing GGA and GGA + U calculations. *Phys. Rev. B - Condens. Matter Mater. Phys.* **84**, 1–10 (2011).

28. Jain, A. *et al.* A high-throughput infrastructure for density functional theory calculations. *Comput. Mater. Sci.* **50**, 2295–2310 (2011).

29. Jain, A. *et al.* Commentary: The materials project: A materials genome approach to accelerating materials innovation. *APL Mater.* **1**, (2013).

Investigation of Sr-based perovskites for redox-type thermochemical energy storage media at medium-high temperature

Xiaoyu Chen[a], Mitsuhiro Kubota[a*], Seiji Yamashita[b], Hideki Kita[a]

[a]Nagoya University, Graduate school of Engineering, Department of Chemical Systems Engineering, Nagoya 4648603, Japan

[b]Nagoya University, Graduate school of Engineering, Department of Materials Process Engineering, Nagoya 4648603, Japan

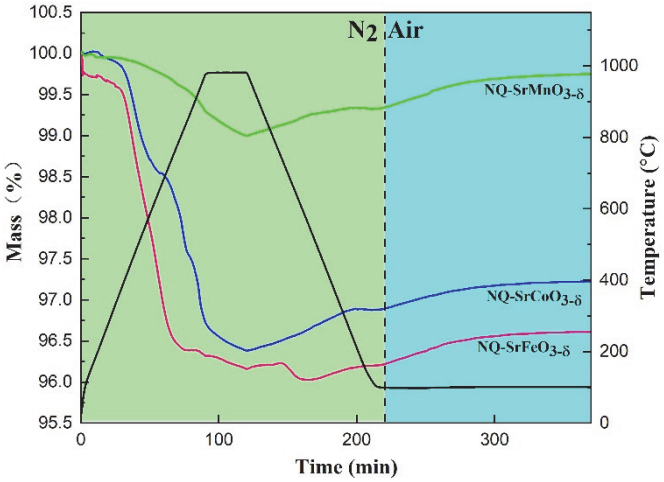

Figure.S1 Oxidation behavior in air at 100 °C for reduced NQ-ABO_3

Table S1. The value of Δδ for NQ-$ABO_{3-\delta}$ reduced in N_2 and oxidation in air at 100°C.

Experiment Condition	NQ-$SrCoO_{3-\delta}$	NQ-$SrFeO_{3-\delta}$	NQ-$SrMnO_{3-\delta}$
Reduction in N_2	0.439	0.459	0.119
Oxidation in air at 100 °C	0.041	0.048	0.049
Re-oxidation temperature	450 °C	400 °C	(-)

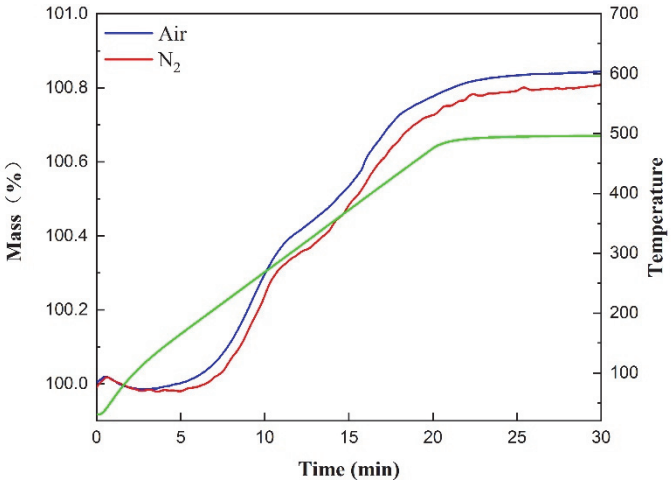

436 **Figure.S2** Oxidation behavior of reduced $SrMnO_{3-\delta}$ in air/N_2 during heating

437

438